Studies of Electromagnetically Induced Transparency in Thallium Vapor and Possible Utility for Measuring Atomic Parity Nonconservation

A. D. Cronin,* R. B. Warrington, S. K. Lamoreaux,† and E. N. Fortson
Department of Physics, P.O. Box 351560, University of Washington, Seattle, Washington 98195
(Received 4 November 1997)

Motivated by the potential use of electromagnetically induced transparency (EIT) to measure atomic parity nonconservation (PNC), we have studied EIT and associated optical rotation for a three-level system in thallium vapor. EIT allows sub-Doppler resolution of the $6P_{1/2} \rightarrow 6P_{3/2}$ mixed magnetic dipole, electric quadrupole transition at 1.28 μm when 0.535-μm radiation acts on the $6P_{3/2} \rightarrow 7S_{1/2}$ transition. Our measurements include rotation due to electromagnetically induced birefringence and Faraday rotation perturbed by EIT. We also identify a new method for determining the amplitude ratio $\mathcal{E}2/\mathcal{M}1$ for the 1.28-μm transition. The possible advantages of an EIT technique for measuring atomic PNC are discussed in the context of our results. [S0031-9007(98)05976-6]

PACS numbers: 32.80.Ys, 11.30.Er, 33.55.–b, 42.50.Gy

After twenty years of development, studies of parity nonconserving (PNC) effects in heavy atoms [1] have reached 1% precision or better [2,3]. At this level, measurements significantly constrain theories of the fundamental electroweak interaction when combined with results obtained at high energies [4]. One such atomic measurement is the 1% determination of PNC optical rotation in thallium (Tl) vapor, on the $6P_{1/2} \rightarrow 6P_{3/2}$ mixed magnetic dipole, electric quadrupole ($M1, E2$) absorption line at 1.28 μm [2]. In principle, the phenomenon of electromagnetically induced transparency (EIT) [5] should allow continued improvement in precision through both sub-Doppler resolution of optical rotation and improved subtraction of background rotations. To this end, we report here a detailed study of EIT and associated optical rotation on the $6P_{1/2} \rightarrow 6P_{3/2}$ transition when transparency is induced by a 0.535-μm laser beam connecting the $6P_{3/2}$ and $7S_{1/2}$ states.

We have studied sub-Doppler absorption and optical rotation features on the 1.28-μm line and the changes in these features caused by an external magnetic field. Doppler-blended hyperfine and Zeeman components can become well resolved in induced transparency, permitting a preliminary measurement of the $\mathcal{E}2/\mathcal{M}1$ amplitude ratio and a detailed study of the effect of Zeeman splitting on EIT. Our results are used below to give an assessment of EIT for a measurement of PNC optical rotation in Tl or other heavy atom vapors, including the importance of a transverse magnetic field to suppress potential systematic birefringent effects.

In previous studies, a three-level system in atomic cesium has been used to achieve sub-Doppler resolution on an $E1$-forbidden optical transition, also with potential application to a PNC measurement [6]. We believe our work is the first use of EIT in this context. EIT refers to the suppression of absorption on an optical transition when a second electromagnetic field is applied on a linked transition. Transparency is induced by the second field primarily (in our case) because the common state is split by the ac Stark effect into two dressed states (an Autler-Townes doublet), reducing absorption on line center. Both the real and imaginary parts of the atomic susceptibility are perturbed so that EIT is accompanied by perturbations to the refractive index, including electromagnetically induced birefringence (EIB) [7,8] and other effects [9,10].

Figure 1 shows the three-level system for the work described here. One laser, the "probe," is scanned across the 1.28-μm absorption, while a second, the "pump," is tuned to the $6P_{3/2} \rightarrow 7S_{1/2}$ transition at 0.535 μm. The pump light generates sharp absorption and rotation features on the probe transition that are much narrower than the Doppler width, because EIT occurs only for atoms in resonance with both laser beams and hence only for a narrow range of velocities along the beam propagation direction.

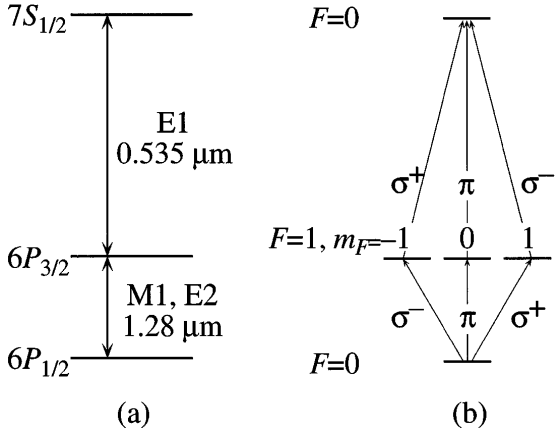

FIG. 1. (a) The three-level system studied in Tl. The hyperfine splitting is 21 GHz for $6P_{1/2}$, 0.5 GHz for $6P_{3/2}$, and 12 GHz for $7S_{1/2}$, with small differences between the two isotopes ^{205}Tl (70.5% abundance, $I = 1/2$) and ^{203}Tl (29.5%, $I = 1/2$). The isotope shift is -0.1 GHz for the 1.28-μm transition and 1.8 GHz at 0.535 μm. (b) Transitions among m_F substates (along an arbitrary quantization axis) for the $F = 0 \rightarrow 1 \rightarrow 0$ EIT channel.

The apparatus is shown in Fig. 2. An external cavity controlled InGaAsP diode laser produces 0.1 mW of continuous wave (cw) 1.28-μm light collimated into a beam of diameter 1 mm in the vapor. An argon ion pumped ring dye laser using Pyrromethene 556 dye produces 50 mW of cw 0.535-μm light collimated into a 2 mm diameter beam that overlaps the probe beam throughout the 0.3-m length of Tl vapor. The vapor is kept at 800 °C in a 1 Torr He buffer gas, producing about 10% peak absorption on the Doppler-broadened $F = 0 \rightarrow 1$ hyperfine component of the 1.28-μm line and larger absorption (not directly involved in EIT) at 0.535 μm due to thermal population of the $6P_{3/2}$ state.

Figure 3 shows the effect of EIT on the transmission profile $T(\nu)$ of the probe beam tuned for absorption by atoms in the $F = 0$ level of the ground state. With the pump off, 3(*a*), the Doppler-broadened absorption has a FWHM of 370 MHz and includes four unresolved components, $F = 0 \rightarrow 1, 2$ for both isotopes. With the pump on, 3(*b*), and tuned to resonance with the $F = 1 \rightarrow 0$ transition of ^{205}Tl atoms at rest in the lab frame, $T(\nu)$ exhibits a well-resolved 50-MHz wide electromagnetically induced transparency. As expected, EIT occurs when the optical *magnetic* field of the probe beam is parallel to the optical *electric* field of the pump beam (perpendicular polarizations), to enable the purely $M1$ 1.28-μm and $E1$ 0.535-μm transitions in the $F = 0 \rightarrow 1 \rightarrow 0$ EIT channel to contact a common m_F level in the intermediate state (see Fig. 1).

Chopping the pump beam at 20 kHz allows the difference spectrum $\Delta T(\nu)$ to be measured with much less noise than by subtraction of full $T(\nu)$ scans. Figure 3(*c*) shows $\Delta T(\nu)$ obtained by this method under similar conditions as 3(*b*) but with four times less pump intensity to reduce power broadening. Figure 3(*d*) is the same scan as 3(*c*), but in a 32 G longitudinal magnetic field that splits the $F = 1$ intermediate state. Just two Zeeman components appear; the $\Delta m = 0$ component is missing because only the $\sigma^{\pm}$ light is present along the longitudinal field axis. The splitting between the Zeeman components in EIT is reduced from the actual splitting in the intermediate state by a factor of 0.42, the ratio of Doppler shifts for the 1.28-μm and 0.535-μm beams.

Transmission profiles computed from a model of EIT are seen to agree well with the data. The model is based on the Schrödinger equation for a three-state atom, assuming weak coupling by the 1.28-μm $M1$, $E2$ transition and arbitrarily strong coupling by the 0.535-μm $E1$ transition. The analytical solution is taken from Ref. [11] for a single velocity class and Doppler convolved numerically. Theoretical curves are fitted to the data with four free parameters, the decay rates $\Gamma(6P_{3/2})$ and $\Gamma(7S_{1/2})$, and the intensity and frequency offset of 0.535-μm light. The Doppler width determined from the measured temperature is used in the convolution and also to calibrate the frequency axis; frequencies calibrated from observed intervals separating Zeeman components or multiple EIT features are consistent. Best-fit decay rates obtained for Fig. 3(*b*) are 1.82×10^8 s^{-1} for $\Gamma(6P_{3/2})$, a reasonable value for collisional broadening of this metastable state, and 3.23×10^8 s^{-1} for $\Gamma(7S_{1/2})$, a sum of collisional broadening and the known radiative decay rate of this state, 1.3×10^8 s^{-1}. Neither decay rate was allowed to float in the subsequent fits 3(*a*), 3(*c*), and 3(*d*). The best-fit Rabi frequency for 3(*b*) is 0.91×10^8 s^{-1}; this value

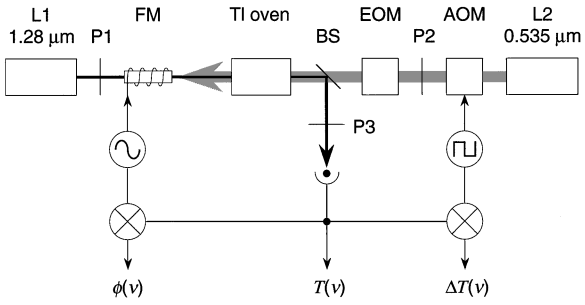

FIG. 2. Experimental apparatus. Counterpropagating beams from lasers L1 and L2 are linearly polarized by calcite polarizers P1 and P2. An electro-optic modulator (EOM) can be used to vary the polarization of the 0.535-μm beam. A dichroic beamsplitter (BS) separates out the 1.28-μm beam, and a photodiode measures the vapor transmission $T(\nu)$. For polarimetry, another polarizer P3 crossed with P1 is added after the Tl oven, and a Faraday modulator (FM) (a glass rod in a field coil) is used to modulate the linear polarization; phase-sensitive detection gives the optical rotation $\phi(\nu)$ [2]. Finally, an acousto-optic modulator (AOM) is used to chop the 0.535-μm beam, and detection at the chop frequency gives the EIT signal $\Delta T(\nu)$. Magnetic field coils are not shown. The effect of BS on the polarization of both beams has been studied in detail and is negligible for data presented here.

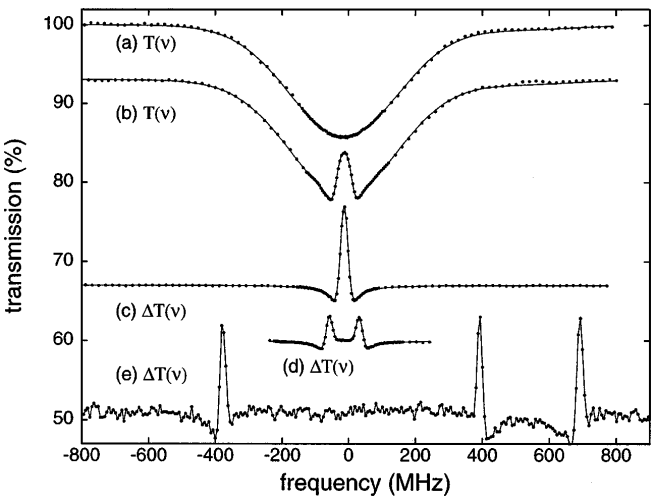

FIG. 3. Transmission line shapes for 1.28-μm transitions from the $6P_{1/2}$ $F = 0$ state on a common frequency axis. The abscissa shows transmission calibrated for curve (*a*); subsequent curves are offset. Curves (*c*) and (*d*) are shown to a different common vertical scale. Fitted model profiles are shown (lines) for curves (*a*)–(*d*); lines on curve (*e*) simply connect data points for clarity.

was halved (to match the reduced pump intensity) and not allowed to float when fitting 3(*c*) and 3(*d*). The 1.28-μm frequency offset was floated in all of the fits to allow for drift in the laser. To incorporate Zeeman splitting, the model is adapted to include the three m_F sublevels of the $F = 1$ intermediate state, with the complex couplings for $\sigma^{\pm}$ and π light indicated in Fig. 1. The only free parameters in fit 3(*d*) were the external magnetic field strength and 1.28-μm frequency offset.

By appropriately tuning the pump frequency to contact the Doppler wings of several 0.535-μm components, it is possible to observe multiple resolved EIT channels. Figure 3(*e*) shows features due to (from left to right) $F = 0 \rightarrow 1 \rightarrow 1$ for ^{203}Tl and ^{205}Tl and $F = 0 \rightarrow 2 \rightarrow 1$ for ^{205}Tl. The first two are pure $M1$ transitions at 1.28 μm while the third is pure $E2$. The three EIT peaks are nearly equal in size because the pump frequency and polarization were chosen to enhance the smaller features.

Although it is possible to use the data in Fig. 3(*e*) to measure the amplitude ratio $\chi \equiv \mathcal{E}_2/\mathcal{M}_1$, it would require accurate modeling of the EIT dependence on pump intensity and detuning in different channels. A much more precise value may be obtained by measuring the ratio of $\Delta T(\nu)$ amplitudes for the $F = 1 \rightarrow 1 \rightarrow 0$ and $F = 0 \rightarrow 1 \rightarrow 0$ channels at several polarizations, so that the coupling of the 0.535-μm light to the $6P_{3/2}$ $F = 1$ state is identical for both channels and cancels in the ratio of the EIT peak heights. This ratio is $(1/4)\,|(3\chi/\sqrt{5}) - 1|^2 \cot^2\alpha$, with α the angle between the two laser polarizations. In a test of this method, we obtained a preliminary value $\chi = 0.22$, where no assessment of systematic uncertainty has been made. This result can be compared to values in the range 0.24 to 0.25 obtained from fitting Doppler broadened $T(\nu)$ and Faraday $\phi(\nu)$ [2,12,13], and to the latest theoretical value 0.24 [14]. Knowledge of χ is important both for analysis of Tl PNC data [2,15] and to confirm atomic theory needed to interpret these measurements; 1% precision seems possible in a dedicated measurement using EIT. The sub-Doppler resolution of the technique eliminates line-shape issues which make precise values difficult to obtain from Doppler-broadened profiles.

For atomic PNC, we are interested primarily in the effects of EIT on optical rotation of the 1.28-μm light, for which the key parameter is $n(\nu)$, the real part of the refractive index. Using the model of EIT above, $n(\nu)$ can be obtained from the Kramers-Kronig transform of the 1.28-μm absorptivity, leading to the familiar antisymmetric dispersion curve for a symmetric absorption feature. When σ^+ light and σ^- light have different indices $n^+(\nu)$ and $n^-(\nu)$, the different phase velocities cause a rotation angle $\phi(\nu) = 2\pi[n^+(\nu) - n^-(\nu)]L/\lambda$ for linearly polarized light in a vapor length L. Differences between $n^+(\nu)$ and $n^-(\nu)$ at 1.28 μm in Tl can be created by a longitudinal magnetic field, by circular polarization in the 0.535-μm light beam, and by parity nonconservation within the atoms.

Figure 4 shows sub-Doppler 1.28-μm optical rotation features due to the $F = 0 \rightarrow 1 \rightarrow 0$ EIT channel. Figure 4(*a*) shows EIT-Faraday rotation with a 32 G longitudinal magnetic field and linearly polarized pump light. $\Delta\phi(\nu)$ has the shape of a Kramers-Kronig transform of the Zeeman absorption pattern in Fig. 3(*d*), but with opposite signs of rotation for the two Zeeman components, and is symmetric overall about the EIT line center. In 4(*b*), when the pump beam is σ^- polarized, EIT only occurs for the σ^+ component of the probe light (as expected from the selection rules of Fig. 1), and the EIT-Faraday rotation appears as an antisymmetric feature at a single EIT-Zeeman peak. The rotation occurs with opposite sign at the other Zeeman peak when the pump beam is σ^+ polarized. The antisymmetric rotation features due to circularly polarized pump light persist in zero magnetic field, as shown in 4(*c*). This dependence of $\Delta T(\nu)$ and $\Delta n(\nu)$ on probe polarization caused by polarization of the pump beam has been named electromagnetically induced birefringence, and observation of EIB optical rotation has been reported previously [7,8]. The rotation at zero field takes on a different line shape with reduced amplitude in a *transverse* magnetic field: 4(*d*) shows EIB rotation in a transverse field of approximately 32 G, with a model curve for a field of 64 G. We have also observed pseudorotations, due to differential absorption of components of the 1.28-μm polarization along either the 0.535-μm linear polarization or an external transverse magnetic field; these can be distinguished from PNC rotation by their line shape and their dependence on the angle of the 1.28-μm polarization.

The model rotation profiles shown in Fig. 4 agree qualitatively with the data shown (here the model parameters

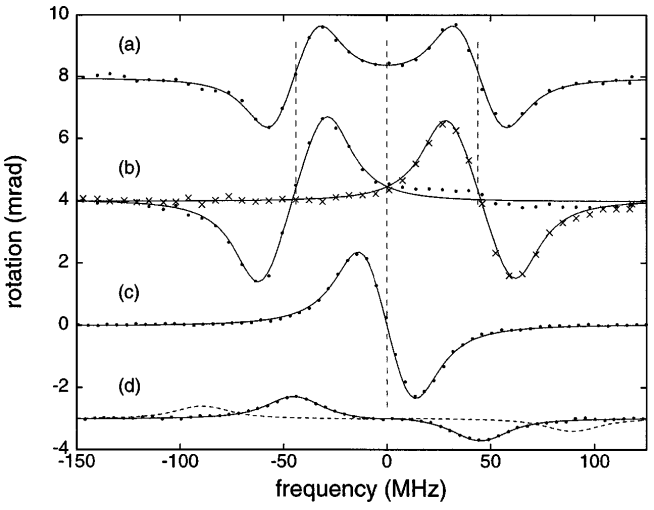

FIG. 4. Observed and modeled rotation line shapes for 1.28-μm transitions from the $6P_{1/2}$ $F = 0$ state on a common frequency axis. The quantity plotted is $\Delta\phi(\nu)$, the change in 1.28-μm rotation when the 0.535-μm beam is turned on. Vertical dashed lines mark the frequencies where Zeeman-split $\Delta T(\nu)$ maxima occur. The pump polarization and magnetic field for each curve are discussed in the text.

have not been optimized by least-squares fitting). Residuals in 4(*b*) may be attributed to ellipticity in the pump light. The model can be improved by adding the mixing of hyperfine states due to the magnetic field and other refinements.

We are now in a position to discuss how EIT could be used to make improved measurements of PNC optical rotation, and also to identify problems that might limit the utility of EIT in such measurements with Tl or other elements. For definiteness, we shall refer to the previous PNC experiment made in this laboratory [2]. Optical rotation arising from the intrinsic atomic chirality, of order 0.1 μrad per absorption length at the peaks of the $n(\nu)$ dispersion curve, was measured on the 1.28-μm absorption line with full Doppler broadening as in Fig. 3(*a*). Frequency-dependent background rotations of the same scale from apparatus imperfections were reduced by comparing rotation profiles recorded both with and without Tl vapor in the optical path of the polarimeter. To improve the precision, two dominant systematic uncertainties must be addressed: drift in the background rotation recorded without Tl vapor over the course of the experiment (10–15 min), and line-shape uncertainties affecting least-squares fitting. The latter include uncertainty in χ and arise because the hyperfine and isotopic components are not individually resolved.

All of these problems can be mitigated by EIT. The EIT rotation feature due to atomic PNC should appear with the exact dispersive shape of Fig. 4(*c*) when the pump beam is linearly polarized, i.e., in the absence of any circular polarization of the 0.535-μm light. This two-laser technique has three principal advantages over the 1.28-μm transition alone. First, sub-Doppler resolution makes background trends less significant. Second, the background spectrum can be obtained by turning off the pump light; chopping this beam and using phase-sensitive detection allows improved sensitivity in the subtraction of background rotations and greatly reduces susceptibility to background drift, since the chopping takes much less time than removing the Tl vapor from the polarimeter beam path. Third, the isotopic and hyperfine components participating in EIT can be examined one at a time by varying the pump frequency, which eliminates the line-shape uncertainties due to overlapping components.

A further advantage of EIT is that measurements obtained for individual components can now be compared. Isotopic components are especially important, since these can be combined to avoid the uncertainty in the atomic theory needed to interpret the experimental results [1]; no PNC measurements comparing individual isotopes have yet been made.

With these advantages of EIT also come some potential limitations to a PNC measurement. Absorption of 0.535-μm light by the thermal population in $6P_{3/2}$ limits the useful Tl vapor density to 0.1 absorption lengths at 1.28 μm, and thus limits the observable PNC rotation. Nevertheless, the method remains quite sensitive; assuming 5 mW of detected 1.28-μm light, the shot noise limited uncertainty would be 0.5% of the peak PNC rotation in a 2 h measurement. A serious systematic problem might be the EIB rotation resulting from even very small residual circular polarization of the 0.535-μm light, which at zero magnetic field has the same shape as $\Delta\phi(\nu)$ due to PNC. One solution to this problem is shown by our studies of EIB rotation in a transverse magnetic field. With the pump beam linearly polarized parallel to an external magnetic field, a large unshifted component of the PNC rotation remains while $\Delta\phi(\nu)$ due to EIB takes on a different line shape with a reduced amplitude, as seen in Fig. 4(*d*). The EIB rotation becomes nearly zero at frequencies where $\Delta\phi(\nu)$ due to PNC is nearly maximum, thus sharply reducing the size of PNC-like features due to any residual circular polarization of the pump light. In addition, the Zeeman-shifted peaks in the EIB profile provide a sensitive detector of birefringence to minimize the residual pump circular polarization.

This work is supported under NSF Grant No. PHY-9506361; A. D. C. acknowledges support under the NSF Graduate Research Fellowship Program. We are grateful to R. Maruyama and P. Vetter for assistance with the experiments, and to F. Pavone and M. Inguscio for a preprint of Ref. [8].

*Corresponding author.
†Current address: Los Alamos National Laboratory, Los Alamos, NM 87545.

[1] M.-A. Bouchiat and C. Bouchiat, J. Phys. (Paris) **35**, 899 (1974); Rep. Prog. Phys. **60**, 1351 (1997).
[2] P. A. Vetter *et al.*, Phys. Rev. Lett. **74**, 2658 (1995).
[3] C. S. Wood *et al.*, Science **275**, 1759 (1997).
[4] J. L. Rosner, Phys. Rev. D **53**, 2724 (1996).
[5] K.-J. Boller, A. Imamoglu, and S. E. Harris, Phys. Rev. Lett. **66**, 2593 (1991); S. E. Harris, Phys. Today **50**, No. 7, 36 (1997).
[6] M. Lintz *et al.*, Europhys. Lett. **4**, 53 (1987); M. A. Bouchiat *et al.*, J. Phys. (France) **50**, 157 (1989).
[7] S. Cavalieri *et al.*, Phys. Rev. A **47**, 4219 (1993).
[8] F. S. Pavone *et al.*, Opt. Lett. **22**, 736 (1997).
[9] S. E. Harris, J. E. Field, and A. Kasapi, Phys. Rev. A **46**, R29 (1992).
[10] R. R. Moseley *et al.*, Phys. Rev. A **53**, 408 (1996).
[11] D. E. Roberts and E. N. Fortson, Phys. Rev. Lett. **31**, 1539 (1973).
[12] N. H. Edwards, S. J. Phipp, and P. E. G. Baird, J. Phys. B **28**, 4041 (1995).
[13] P. K. Majumder (private communication).
[14] A. M. Martensson-Pendrill (private communication).
[15] N. H. Edwards, S. J. Phipp, P. E. G. Baird, and S. Nakayama, Phys. Rev. Lett. **74**, 2654 (1995).